

Water Oxidation Catalyzed by Cobalt(II) Adsorbed on Silica Nanoparticles

Tomer Zidki,[†] Lihua Zhang,[‡] Vladimir Shafirovich,[§] and Sergei V. Lymar*,[†]

[†]Chemistry Department and [‡]Center for Functional Nanomaterials, Brookhaven National Laboratory, Upton, New York 11973, United States

[§]Chemistry Department, New York University, New York, New York 10003, United States

S Supporting Information

ABSTRACT: A novel, highly efficient, and stable water oxidation catalyst was prepared by a pH-controlled adsorption of Co(II) on ~10 nm diameter silica nanoparticles. A lower limit of ~300 s⁻¹ per cobalt atom for the catalyst turnover frequency in oxygen evolution was estimated, which attests to a very high catalytic activity. Electron microscopy revealed that cobalt is adsorbed on the SiO₂ nanoparticle surfaces as small (1–2 nm) clusters of Co(OH)₂. This catalyst is optically transparent over the entire UV–vis range and is thus suitable for mechanistic investigations by time-resolved spectroscopic techniques.

Here we report a novel, efficient, stable, and optically transparent catalyst for oxidation of water to molecular oxygen based on cobalt(II) adsorbed on silica nanoparticles. Water oxidation catalyzed by Co(II) either on an anode¹ or in the bulk with a strong one-electron oxidant (e.g., IrCl₆²⁻ or a bipyridine complex of trivalent Ru, Fe, or Os) produced photochemically² in situ or by chemical oxidation^{2a,b,3} was reported almost 35 years ago. In spite of high initial activity, that catalyst was rapidly deactivated as a result of extensive Co hydrolysis and precipitation as Co(II) or Co(III) hydroxides produced during catalytic cycling.^{3b,c} At about the same time, it was shown that the Co catalyst maintains its catalytic activity upon stabilization by organic matrices (lipid bilayers⁴ or cyclodextrins⁵) or precipitation on powdered silica, alumina, and other oxides,⁶ which render the catalyst heterogeneous.

Interest in Co hydroxide/oxide-based water oxidation catalysis has been rekindled along with a surge in research toward solar energy utilization, and a number of new catalysts of this kind have been introduced.⁷ Most of these catalysts are macroheterogeneous and thus either opaque or highly light-scattering, which makes the use of spectroscopic techniques for their mechanistic investigation difficult. Under certain conditions, mass transfer, particularly of the oxidant to the catalytic center, may become rate-determining, obscuring the catalysis itself. To mitigate these problems, we turned to silica nanoparticles, whose role is to guard Co against precipitation in all oxidation states that might be involved in a catalytic cycle and provide a highly dispersed, optically transparent, soluble system.

The catalysts were prepared by pH-jump flow mixing of solutions of alkaline ~10 nm silica nanoparticles and acidic Co(II). When the concentration of Co(II) exceeded its

solubility at the mixture pH, a blue Co(OH)₂ precipitate was promptly formed in the absence of silica. In contrast, no Co(OH)₂ precipitation was observed with silica; a pale-pink sample solution formed and was indefinitely stable toward precipitation, remaining clear and homogeneous both at natural gravity and under centrifugation at 5000g [Figure S1 in the Supporting Information (SI)]. These results indicated that Co(II) was adsorbed on the silica nanoparticles. This conclusion was corroborated by measurements of Co recovery after the sample solutions with and without silica nanoparticles were passed through a 0.22 μm filter (Table S1 in the SI). At alkaline pH (9.1–9.7), over 95% of the Co passed through the filter when silica was added, while less than 1% of the Co was recovered in the filtrate in the absence of silica. Thus, adsorption on silica nanoparticles stabilizes Co(II) against the formation of macroscopic Co(OH)₂ solid aggregates and attendant precipitation.

The Co(II) adsorption was investigated by pressure-assisted ultrafiltration through a 10 kDa cutoff polyethersulfone membrane that was impermeable to silica nanoparticles (Table S2). The results in Figure 1 show that the Co(II) adsorption was strongly pH-dependent, rapidly increasing in the narrow pH range from 6 to 8 and reaching 100% just above pH 9. This behavior resembles the pH dependence of Co(II) adsorption on crushed α-quartz.⁸ A detailed investigation of Co adsorption on silica nanoparticles will be reported elsewhere. Here it is sufficient to note that this process is more complex than merely Co(II) hydrolysis followed by precipitation of poorly soluble Co(OH)₂ on an inert substrate. Indeed, the data in Figure 1 reveal little correlation between the Co(II) adsorption and its solubility: first, adsorption began at much lower pH than precipitation of Co(OH)₂, and second, silica nanoparticles scavenged even the soluble fraction of Co(OH)₂ at high pH.

The adsorption morphology is illustrated in Figure 2, which reveals that the adsorbed Co(II) aggregates in small (1–2 nm diameter) clusters scattered over the silica particle surface. Considering the sample preparation conditions and the apparent aggregation, we believe that the clusters consist of Co(OH)₂. From the Co loading of 360 atoms per silica particle and the average number of 15 clusters per particle in Figure 2, we estimate that each cluster contains on average about 25 Co atoms. This estimate coincides with the number of Co(OH)₂

Received: May 9, 2012

Published: August 22, 2012

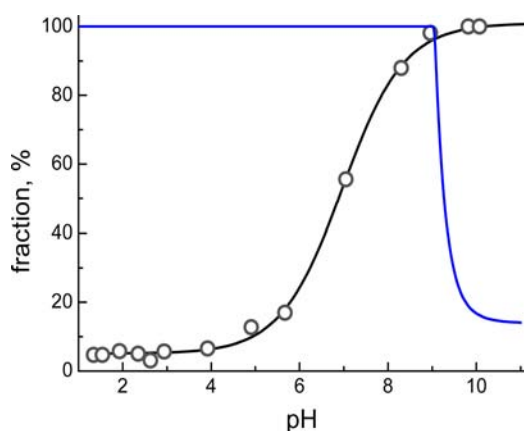


Figure 1. pH dependence of the fraction of added Co(II) adsorbed on silica (O) and a sigmoidal fit to the data (black curve). Conditions: 72 μM Co(II), 89 mM SiO_2 ; the pH was adjusted with H_2SO_4 , NaOH, acetate, phosphate, and borate buffers while maintaining $[\text{Na}^+]$ constant at 4.6 mM. The blue curve shows the Co(II) solubility calculated from Co hydrolysis data compiled by Bayes and Mesmer⁹ and Smith and Martell.¹⁰ The solubility is expressed as the fraction of added Co(II) that remains dissolved [i.e., sum of Co^{2+} , $\text{Co}(\text{OH})^+$, and $\text{Co}(\text{OH})_2$ molecular species] at a given pH; the balance precipitates as solid $\text{Co}(\text{OH})_2$.

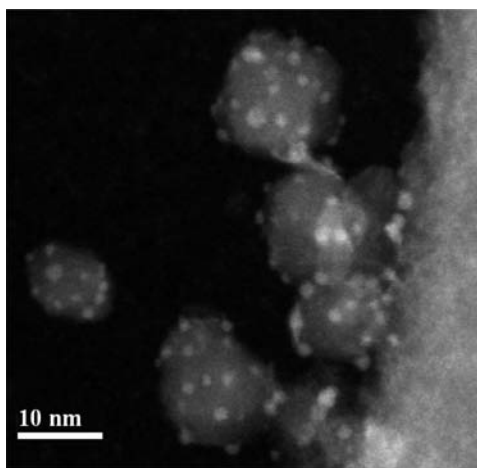
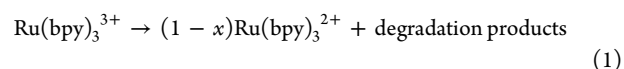


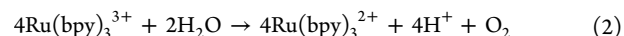
Figure 2. High-angle annular dark-field scanning transmission electron microscopy image of silica nanoparticles (~ 10 nm gray spherical objects) with adsorbed Co(II). The higher-Z-contrast, Co-rich areas are seen as the brighter 1–2 nm spots scattered over the surfaces of the SiO_2 nanoparticles. The presence of Co in these spots was confirmed by energy-dispersive and electron energy loss spectroscopies. The sample contained 12 mM SiO_2 and 0.37 mM Co(II) at pH 9, which corresponds to 360 Co atoms per 10 nm particle on average.

units in a 1.5 nm spherical crystalline Co(II) hydroxide cluster. For a cluster this size, most if not all of the $\text{Co}(\text{OH})_2$ units are on the cluster surface and available for reacting with solutes in the surrounding medium.

Water oxidation catalysis was investigated using tris(2,2'-bipyridine)ruthenium(III), $\text{Ru}(\text{bpy})_3^{3+}$, as a one-electron oxidant [$E^0(\text{Ru}^{3+/2+}) = 1.26$ V vs NHE];¹¹ the oxidant was prepared as described previously.¹² In the absence of a catalyst, $\text{Ru}(\text{bpy})_3^{3+}$ undergoes a spontaneous reduction that is accompanied by oxidative degradation of a small fraction of the complex,



with $x < 0.05$,^{3b,d,12} without participating in the water oxidation reaction



To achieve water oxidation with $\text{Ru}(\text{bpy})_3^{3+}$, a catalyst is required for which the rate of reaction 2 (v_2) is much greater than the rate of reaction 1 (v_1). In addition to being catalyst-dependent, both rates are also medium-dependent, especially with respect to pH.

Oxygen yields were measured using a syringe-driven anaerobic mixing system equipped with a headspace-free flow cell and a Clark-type oxygen probe. The oxygen yield data in Figure 3 demonstrate the high selectivity of the catalyst: even at

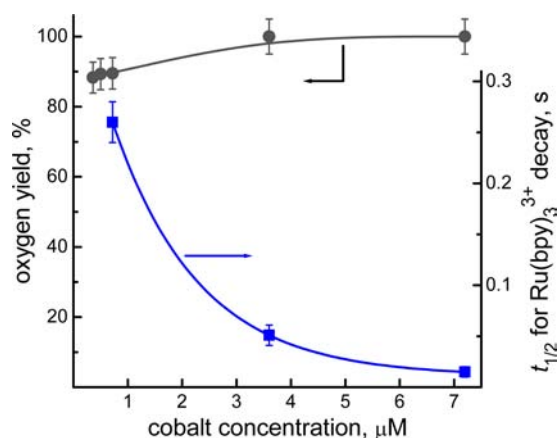


Figure 3. Dependences on the concentration of $\text{Co}(\text{OH})_2/\text{SiO}_2$ catalyst in 10 mM borate at pH 9.4. Left axis (circles): oxygen yield based on the stoichiometry of reaction 2. Concentrations of added $\text{Ru}(\text{bpy})_3^{3+}$ were in the 0.24–0.34 mM range. Right axis (squares): half-life for the consumption of $\text{Ru}(\text{bpy})_3^{3+}$ (from Figure S2); in the absence of catalyst, $t_{1/2} = 3.4$ s was measured. To maintain constant Co per particle loading, the $[\text{Co}(\text{II})]/[\text{SiO}_2]$ ratio was kept constant at 8×10^{-3} .

submicromolar Co concentrations, the yield was close to 90% of that expected from reaction 2, and it reached 100% at several micromolar catalyst concentrations. Notably, the Co catalyst did not promote oxidative degradation of the ligands in $\text{Ru}(\text{bpy})_3^{3+/2+}$, as do the oxides/hydroxides of noble metals such as RuO_2 .¹³

The nearly 100% yield of oxygen implies that $v_2 \gg v_1$, allowing the catalyst activity to be measured from the $\text{Ru}(\text{bpy})_3^{3+}$ reduction; that is, $4d[\text{O}_2]/dt = -d[\text{Ru}(\text{bpy})_3^{3+}]/dt$. As in the O_2 evolution experiments described above, the acidic oxidant and alkaline catalyst solutions were mixed, and the decay kinetics of $\text{Ru}(\text{bpy})_3^{3+}$ were recorded by the stopped-flow technique at the 675 nm absorption band of $\text{Ru}(\text{bpy})_3^{3+}$ ($\epsilon_{\text{max}} = 420 \text{ M}^{-1} \text{ cm}^{-1}$).¹¹ The results in Table 1 and Figure S2 show that $\text{Ru}(\text{bpy})_3^{3+}$ decay was strongly accelerated by the $\text{Co}(\text{OH})_2/\text{SiO}_2$ catalyst in a concentration-dependent manner. The decays were exponential for at least 80% of the kinetics, and the corresponding half-lives are plotted in Figure 3. The first-order $\text{Ru}(\text{bpy})_3^{3+}$ decay kinetics suggests that the rate-determining step in water oxidation is the reaction between the catalyst and the oxidant. Comparison of the k values in Table 1 with the value $k \approx 1.5 \times 10^6 \text{ M}^{-1} \text{ s}^{-1}$ that we estimated from data previously obtained for an unsupported Co catalyst under

Table 1. Stopped-Flow Rate Data for the Catalytic Consumption of Ru(bpy)₃³⁺ in Reaction 2 at pH 9.4, 10 mM Borate, 25 °C

[Co(II)] (μM) ^a	[Ru(III)] ₀ (mM) ^b	initial rate (mM s ⁻¹) ^c	10 ⁻⁶ × <i>k</i> (M ⁻¹ s ⁻¹) ^d	yield of Co(III) ^e
0	0.20	0.05		
0.72	0.21	0.79	5.2	1.0
3.6	0.22	3.6	4.6	0.93
7.2	0.17	9.7	7.7	0.98

^aThe [Co(II)]/[SiO₂] ratio was kept constant at 8 × 10⁻³. ^bInitial concentration of Ru(bpy)₃³⁺. ^cFor [Co(II)] > 0, the rates were corrected for uncatalyzed Ru(bpy)₃³⁺ decay at a rate of 0.05 mM/s according to reaction 1. ^dApparent rate constant, defined as the ratio of initial rate to the product [Co(II)] × [Ru(III)]₀. ^eEnd-of-reaction yield ([Co(III)]_{final}/[Co(II)]_{initial}) determined from the residual absorptions (Figure S2) and the Co(III) spectrum (Figure S3).

very similar conditions^{3b} (pH 9.2, [Co(II)] = 0.5–5 μM, [Ru(III)]₀ = 0.5 mM) shows that Co adsorption on silica not only does not impede but even somewhat increases the catalytic activity.

The initial Co turnover frequencies (TOFs) with respect to oxygen evolution (TOF = initial rate/4[Co(II)]) were estimated from the data in Table 1 to be ~300 s⁻¹. Since they are dependent on the oxidant concentration, these numbers represent the *lower limits* of the TOF the catalyst is capable of reaching. Comparing these limits with the TOF values compiled by Styring and co-workers⁷¹ for a number of Co-based water oxidation catalysts, none of which exceeds 0.3 s⁻¹, we conclude that we have a very active catalyst.

Residual absorptions that increase with the catalyst concentration were observed at 675 nm after complete consumption of Ru(bpy)₃³⁺ (Figure S2). Because the Ru(bpy)₃²⁺ product does not absorb at this wavelength, we interpret this residual absorption as due to conversion of Co(II) to Co(III) during water oxidation catalysis. This suggestion was borne out by the observation that such absorption appeared upon exposure of the catalyst to γ radiation in an N₂O-saturated solution (Figure S3). Under these conditions, the major water radiolysis product is the OH radical, which readily oxidizes Co(II) according to the reaction Co(OH)₂ + OH → Co(OH)₃.¹⁴ The last column in Table 1 shows that the Co(III) yields calculated from the residual absorption amplitudes and the radiolysis data correspond to nearly quantitative conversion of Co(II) to Co(III). Taken together, these observations suggest that Co(III) is the resting catalyst oxidation state.

Multiple water oxidation cycles are shown in Figure 4. In these experiments, the Ru(bpy)₃³⁺ oxidant was generated photochemically using the Ru(bpy)₃²⁺/persulfate system. The oxidant was promptly produced by 355 nm laser pulses according to the overall process 2Ru(bpy)₃²⁺ + S₂O₈²⁻ + hν → 2Ru(bpy)₃³⁺ + 2SO₄²⁻,¹⁵ and oxygen evolution was observed in parallel with the oxidant decay. Without added catalyst, practically no prominent oxygen signal on top of the slow system leakage was observed. However, in the presence of the Co(OH)₂/SiO₂ catalyst, oxygen evolution was detected in response to each laser pulse. The nearly linear oxygen accumulation and constancy of the amplitudes for individual steps were observed all the way to the oxygen solubility limit. These results suggest that little, if any, catalyst deactivation and/or Ru(bpy)₃^{2+/3+} degradation occurs during repetitive water oxidation cycles, attesting to the high catalyst stability.

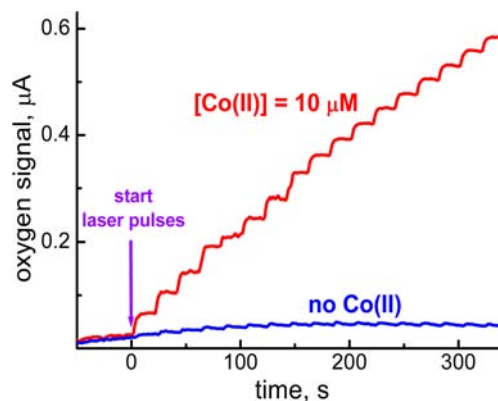


Figure 4. Accumulation of oxygen upon repetitive 355 nm laser pulsing at 0.05 Hz in the absence (lower trace) or the presence (upper trace) of the Co(OH)₂/SiO₂ catalyst with [Co(II)] = 10 μM and [SiO₂] = 1 mM. Each step corresponds to a single laser pulse generating 25–30 μM Ru(bpy)₃³⁺ oxidant. Conditions: 10 mM borate at pH 9.0, 100 μM Ru(bpy)₃²⁺, 10 mM S₂O₈²⁻.

In summary, we have introduced a novel approach for the synthesis of an all-inorganic, high-surface-area, heterogeneous yet soluble catalyst for water oxidation with one-electron oxidants. This approach involves adsorption of Co(II) on oxide (in this particular case, silica) nanoparticles with attendant formation of 1–2 nm Co(II) hydroxide clusters. The Co(OH)₂/SiO₂ catalyst demonstrates both high selectivity and catalytic activity in water oxidation by a classical one-electron oxidant, Ru(bpy)₃³⁺. The catalyst also shows high stability; no deactivation or cobalt precipitation was observed upon multiple cycling of Co ions through their higher (III and, most probably, IV) oxidation states that must be involved in the water oxidation process. This catalyst is optically transparent over the entire UV–vis range and is suitable for further mechanistic investigations by time-resolved spectroscopic techniques such as stopped flow, flash photolysis, and pulse radiolysis, which are now in progress.

■ ASSOCIATED CONTENT

📄 Supporting Information

Experimental procedures and catalyst characterization data, including photographs, tables, and UV–vis spectra. This material is available free of charge via the Internet at <http://pubs.acs.org>.

■ AUTHOR INFORMATION

Corresponding Author

lymar@bnl.gov

Notes

The authors declare no competing financial interest.

■ ACKNOWLEDGMENTS

This work and the use of TEM facilities at the BNL Center for Functional Nanomaterials and the Co-60 source at the BNL Accelerator Center for Energy Research were supported by the U.S. Department of Energy (DOE), Office of Basic Energy Sciences (BES), Division of Chemical Sciences, Geosciences, and Biosciences, under Contract DE-AC02-98CH10886. The authors also thank DOE for funding under the BES Hydrogen Fuel Initiative; Drs. Norman Sutin, Carol Creutz, and James Hurst for insightful advice; and Nissan Chemicals Inc. for providing free samples of colloidal silica.

■ REFERENCES

- (1) Shafirovich, V. Y.; Strelets, V. V. *Nouv. J. Chim.* **1978**, *2*, 199.
- (2) (a) Shafirovich, V. Y.; Khannanov, N. K.; Strelets, V. V. *Nouv. J. Chim.* **1980**, *4*, 81. (b) Shafirovich, V. Y.; Khannanov, N. K.; Strelets, V. V. *Dokl. Akad. Nauk SSSR* **1980**, *250*, 1197. (c) Khannanov, N. K.; Shafirovich, V. Y. *Dokl. Akad. Nauk SSSR* **1981**, *260*, 1418.
- (3) (a) Khannanov, N. K.; Shafirovich, V. Y. *Kinet. Katal.* **1981**, *22*, 248. (b) Khannanov, N. K.; Khranov, A. V.; Moravskii, A. P.; Shafirovich, V. Y. *Kinet. Katal.* **1983**, *24*, 858. (c) Bruntschwig, B. S.; Chou, M. H.; Creutz, C.; Ghosh, P.; Sutin, N. *J. Am. Chem. Soc.* **1983**, *105*, 4832. (d) Ghosh, P. K.; Bruntschwig, B. S.; Chou, M.; Creutz, C.; Sutin, N. *J. Am. Chem. Soc.* **1984**, *106*, 4772.
- (4) (a) Knerel'man, E. I.; Shafirovich, V. Y. *Kinet. Katal.* **1987**, *28*, 1237. (b) Knerel'man, E. I.; Luneva, N. P.; Shafirovich, V. Y.; Shilov, A. E. *Dokl. Akad. Nauk SSSR* **1988**, *299*, 388. (c) Luneva, N. P.; Shafirovich, V. Y.; Shilov, A. E. *New J. Chem.* **1989**, *13*, 107.
- (5) (a) Luneva, N. P.; Shafirovich, V. Y.; Shilov, A. E. *Kinet. Katal.* **1989**, *30*, 250. (b) Luneva, N. P.; Shafirovich, V. Y.; Shilov, A. E. *J. Mol. Catal.* **1989**, *52*, 49.
- (6) (a) Elizarova, G. L.; Kim, T. V.; Matvienko, L. G.; Parmon, V. N. *React. Kinet. Catal. Lett.* **1986**, *31*, 455. (b) Elizarova, G. L.; Matvienko, L. G.; Lozhkina, N. V.; Parmon, V. N. *React. Kinet. Catal. Lett.* **1988**, *36*, 331. (c) Elizarova, G. L.; Zhidomirov, G. M.; Parmon, V. N. *Catal. Today* **2000**, *58*, 71.
- (7) For recent leading references and reviews, see: (a) Kanan, M. W.; Nocera, D. G. *Science* **2008**, *321*, 1072. (b) Jiao, F.; Frei, H. *Angew. Chem., Int. Ed.* **2009**, *48*, 1841. (c) Lutterman, D. A.; Surendranath, Y.; Nocera, D. G. *J. Am. Chem. Soc.* **2009**, *131*, 3838. (d) Kanan, M. W.; Surendranath, Y.; Nocera, D. G. *Chem. Soc. Rev.* **2009**, *38*, 109. (e) Surendranath, Y.; Dincă, M.; Nocera, D. G. *J. Am. Chem. Soc.* **2009**, *131*, 2615. (f) Gerken, J. B.; Landis, E. C.; Hamers, R. J.; Stahl, S. S. *ChemSusChem* **2010**, *3*, 1176. (g) Gerken, J. B.; McAlpin, J. G.; Chen, J. Y.; Rigsby, M. L.; Casey, W. H.; Britt, R. D.; Stahl, S. S. *J. Am. Chem. Soc.* **2011**, *133*, 14431. (h) Wee, T. L.; Sherman, B. D.; Gust, D.; Moore, A. L.; Moore, T. A.; Liu, Y.; Scaiano, J. C. *J. Am. Chem. Soc.* **2011**, *133*, 16742. (i) Shevchenko, D.; Anderlund, M. A.; Thapper, A.; Styring, S. *Energy Environ. Sci.* **2011**, *4*, 1284. (j) Huang, Z. Q.; Luo, Z.; Geletii, Y. V.; Vickers, J. W.; Yin, Q. S.; Wu, D.; Hou, Y.; Ding, Y.; Song, J.; Musaev, D. G.; Hill, C. L.; Lian, T. Q. *J. Am. Chem. Soc.* **2011**, *133*, 2068. (k) Stracke, J. J.; Finke, R. G. *J. Am. Chem. Soc.* **2011**, *133*, 14872. (l) Higashi, M.; Domen, K.; Abe, R. *J. Am. Chem. Soc.* **2012**, *134*, 6968. (m) Tanaka, S.; Annaka, M.; Sakai, K. *Chem. Commun.* **2012**, *48*, 1653. (n) Gardner, G. P.; Go, Y. B.; Robinson, D. M.; Smith, P. F.; Hadermann, J.; Abakumov, A.; Greenblatt, M.; Dismukes, G. C. *Angew. Chem., Int. Ed.* **2012**, *51*, 1616. (o) Risch, M.; Klingman, K.; Ringleb, F.; Chernev, P.; Zaharieva, I.; Fisher, A.; Dau, H. *ChemSusChem* **2012**, *5*, 542. (p) Artero, V.; Chavarot-Kerlidou, M.; Fontecave, M. *Angew. Chem., Int. Ed.* **2011**, *50*, 7238. (q) Sartorel, A.; Carraro, M.; Toma, F. M.; Prato, M.; Bonchio, M. *Energy Environ. Sci.* **2012**, *5*, 5592. (r) Du, P.; Eisenberg, R. *Energy Environ. Sci.* **2012**, *2012*, 6012.
- (8) James, R. O.; Healy, T. W. *J. Colloid Interface Sci.* **1972**, *40*, 42.
- (9) Baes, C. F.; Mesmer, R. E. *The Hydrolysis of Cations*; Wiley-Interscience: New York, 1976.
- (10) Smith, R. M.; Martel, A. E. *Critical Stability Constants*; Plenum Press: New York, 1976; Vol. 4.
- (11) Creutz, C.; Sutin, N. *Proc. Natl. Acad. Sci. U.S.A.* **1975**, *72*, 2858.
- (12) Shafirovich, V. Y.; Khannanov, N. K.; Shilov, A. E. *J. Inorg. Biochem.* **1981**, *15*, 113.
- (13) Shafirovich, V. Y.; Strelets, V. V. *Nouv. J. Chim.* **1982**, *23*, 1311.
- (14) Buxton, G. V.; Sellers, R. M.; McCracken, D. R. *J. Chem. Soc., Faraday Trans. I* **1976**, *72*, 1464.
- (15) (a) Bolletta, F.; Juris, A.; Maestri, M.; Sandrini, D. *Inorg. Chim. Acta* **1980**, *1980*, L175. (b) White, H. S.; Becker, W. G.; Bard, A. J. *J. Phys. Chem.* **1984**, *88*, 1840.